Research article

Integrated profiling identifies ferredoxin 1 as an immune-related biomarker of malignant phenotype in glioma

Dongcheng Xie [a], Hailong Huang [a], Youwei Guo [a], Zhipeng Jiang [a], Yirui Kuang [a], Haoxuan Huang [a], Weidong Liu [b,c], Lei Wang [b,c], Zhaoqi Xin [a,****], Binbin Wang [d,***], Caiping Ren [b,c,**], Xingjun Jiang [a,*]

[a] Department of Neurosurgery, Xiangya Hospital, Central South University, Changsha, China
[b] Cancer Research Institute, School of Basic Medical Science, Central South University, Changsha, China
[c] The NHC Key Laboratory of Carcinogenesis and The Key Laboratory of Carcinogenesis and Cancer Invasion of the Chinese Ministry of Education, Central South University, Changsha, China
[d] Department of Neurosurgery, The First Affiliated Hospital with Nanjing Medical University, 300 Guangzhou Road, Nanjing, China

ARTICLE INFO

ABSTRACT

Background: Glioma, a highly resistant and recurrent type of central nervous system tumor, poses a significant challenge in terms of effective drug treatments and its associated mortality rates. Despite the discovery of Ferredoxin 1 (FDX1) as a crucial participant in cuproptosis, an innovative mechanism of cellular demise, its precise implications for glioma prognosis and tumor immune infiltration remain inadequately elucidated.
Methods: To analyze pan-cancer data, we employed multiple public databases. Gene expression evaluation was performed using tissue microarray (TMA) and single-cell sequencing data. Furthermore, four different approaches were employed to assess the prognostic importance of FDX1 in glioma. We conducted the analysis of differential expression genes (DEGs) and Gene Set Enrichment Analysis (GSEA) to identify immune-related predictive signaling pathways. Somatic mutations were assessed using Tumor Mutation Burden (TMB) and waterfall plots. Immune cell infiltration was evaluated with five different algorithms. Furthermore, we performed in vitro investigations to evaluate the biological roles of FDX1 in glioma.
Results: Glioma samples exhibited upregulation of FDX1, which in turn predicted poor prognosis and was positively associated with unfavorable clinicopathological characteristics. Notably, the top four enriched signaling pathways were immune-related, and the discovery revealed a connection between the expression of FDX1 and the frequency of mutations or the TMB. The FDX1_high group exhibited heightened infiltration of immune cells, and there existed a direct association between the expression of FDX1 and the regulation of immune checkpoint. In vitro experiments demonstrated that FDX1 knockdown reduced proliferation, migration, invasion and transition from G2 to M phase in glioma cells.

* Corresponding authors.
** Corresponding author. Cancer Research Institute, School of Basic Medical Science, Central South University, Changsha, China.
*** Corresponding authors.
**** Corresponding author.
E-mail addresses: xinzhaoqi@csu.edu.cn (Z. Xin), wbbjsph@163.com (B. Wang), rencaiping@csu.edu.cn (C. Ren), jiangxj@csu.edu.cn, jxjyjz@163.com (X. Jiang).

Conclusion: In glioma, FDX1 demonstrated a positive association with the advancement of malignancy and changes in the infiltration of immune cells.

1. Introduction

Gliomas are highly drug-resistant with high recurrence and mortality rates [1–3]. Glioblastoma (GBM) is a type of high-grade glioma that can develop from a low-grade glioma (LGG) [4,5]. Despite the existence of a diverse range of therapeutic alternatives, the prognosis remains unfavorable for individuals diagnosed with glioma, especially for those who have GBM, with more than 90% of patients surviving within five years of diagnosis [6,7]. Biomarkers, such as IDH mutations, co-selection of 1p and 19q chromosomes, and methylation of the MGMT promoter, are associated with glioblastoma prognosis [1]. Therefore, it is essential to search for additional potential prognostic biomarkers to gain insight into the formation mechanisms.

Copper (Cu) serves as a cofactor for crucial enzymes in both animal cells and bacteria, and its presence is linked to the development, incidence, and prognosis of malignant tumors in humans [8]. In comparison with healthy individuals, 60% of breast cancer patients have elevated copper levels [9]. In hepatocellular carcinoma, severe disruption of mitochondrial homeostasis by DSF/Cu leads to increased iron storage, lipid peroxidation, and ultimately ferroptosis [10]. The process of copper-related cell death may potentially contribute to tumor development. The *FDX1* gene encodes a small iron-sulfur protein, which engages in the transfer of electrons from NADPH to mitochondrial cytochrome P450 via ferredoxin reductase. Moreover, the metabolic processes of steroids, vitamin D, and bile acids are regulated by FDX1 [11]. FDX1 serves as a crucial factor in enhancing protein lipidation and is also implicated in the induction of cell death caused by copper [12]. FDX1 regulates the mitochondrial electron transport chain and metabolism and can affect lung adenocarcinoma prognosis [13]. Additionally, the regulation of the TP73 by FDX1 occurs via IRP2, potentially implicating its involvement in both human melanoma and lymphoproliferative diseases [14–16]. Currently, there is limited understanding of how FDX1 expression is modulated in gliomas, its potential prognostic role, its correlation with the tumor microenvironment, and how copper regulation influences glioma through FDX1.

In this study, data was collected from several public databases, clinical and experimental data. We examined the relationship between the FDX1 gene and clinical features in glioma. We also investigated how FDX1 may affect the infiltration of immune cells in glioma. Our findings indicate that when FDX1 is suppressed, there is a reduction in glioma cell proliferation, migration, and invasion. We also observed changes in the cell cycle. These results highlight the importance of FDX1 in the development and progression of glioma.

2. Materials and methods

2.1. Data preparation

The Cancer Genome Atlas (TCGA) and Chinese Glioma Genome Atlas (CGGA) provided the necessary RNA sequence and clinical data of patients. For training purposes, the TCGA database (n = 694) was utilized, while the CGGA database (n = 325) served as the validation dataset. To enrich our analysis, the GTEx database, maintained by the National Institutes of Health's Common Fund, supplied RNA-seq transcriptome data from healthy human tissues. Furthermore, to augment our findings, the European Genome-phenome Archive (EGA) granted us access to the single-cell sequencing data of 55284 cells from 11 glioma patients under the accession number EGAS00001005300, as conducted by Johnson, Kevin C et al. [17]. Subsequently, the raw data was analyzed using the Seurat R package in R studio.

2.2. FDX1 differential expression

In the study conducted by TCGA, we analyzed the expression of FDX1 in 32 distinct tumor types along with their corresponding normal samples. Furthermore, we assessed the FDX1 expression in glioma samples by incorporating data from the GTEx database. To categorize the glioma samples effectively, we segregated them into two groups according to the median mRNA expression level of FDX1.

2.3. Immunohistochemistry

The TMA technology was used to explored FDX1 expression. The Human Ethics Committee of Xiangya Hospital approved all the samples used, and we got the informed consent from all patients involved. The primary antibody against FDX1 (1:100, Proteintech, 12592-1-AP) was incubated overnight, followed by the addition of secondary antibodies conjugated to horseradish peroxidase (1:400, Abcam, USA) for 30 min at 37 °C.

2.4. Survival analysis

We excluded samples that did not have clinical characteristics and those with an overall survival (OS) of less than 30 days. Survival

analysis was conducted by "survminer" and "survival" packages. Kaplan-Meier analysis was performed on three measures of survival: OS, disease-specific survival (DSS), and progression-free interval (PFI). These analyses were done on both the TCGA cohort and validated in the CGGA_325 cohort. The correlation between FDX1 and various important clinical features, such as WHO grade, age, IDH status, 1p/19q codeletion, radiotherapy, and chemotherapy, was investigated in the TCGA and CGGA_325 cohorts. To determine statistical significance, log-rank analysis was employed with a significance threshold set at 0.05.

2.5. Establishment of FDX1-related prognostic model

To assess the impact of FDX1 subgroups and clinical characteristics, such as WHO grade, gender, age, IDH status, 1p/19q code-letion, radiotherapy, and chemotherapy, we conducted univariate Cox regression analysis. The cut-off for determining significance was $p < 0.05$. Furthermore, the selected features were utilized to predict survival via the utilization of a nomogram and multivariate Cox analysis, employing the "rms" package. To assess the reliability of the prognostic model, a calibration curve was employed. Furthermore, the Kaplan-Meier survival analysis and the time-dependent receiver operating characteristic (ROC) curve were applied to compare the RiskScore-H and RiskScore-L in TCGA. Importantly, all analyses were subsequently validated in the CGGA_325 cohort.

2.6. PCA analysis and DEGs analysis

In the TCGA cohort, glioma samples underwent a principle component analysis (PCA). To determine the DEGs between the FDX1_high and FDX1_low groups in TCGA, the "DESeq2" (version 1.26.0) package was employed by conducting an unpaired Student's t-test. Significance was established by an adjusted p-value of less than 0.05 and an absolute log2 fold change greater than 2.0. Visual representation of these DEGs was achieved through a volcano plot, wherein the top 10 up-regulated and 5 down-regulated DEGs were annotated.

2.7. Analysis of functional enrichment

In order to assess the biological pathways associated with the DEGs, we utilized the "clusterProfiler" package. Gene Ontology (GO) categories were used to evaluate cellular components (CC), biological processes (BP), and molecular function (MF), as well as the Kyoto Encyclopedia of Genes and Genomes (KEGG). Additionally, we conducted GSEA analysis using GSEA software version 3.0 to evaluate gene set enrichment (GSE) for each sample in TCGA, comparing FDX1_high and FDX1_low groups. Significance was established using the following criteria: adjusted P-value (p.adj) < 0.05, false discovery rate (FDR) < 0.25, and absolute value of normalized enrichment score (NES) > 1.

2.8. Somatic mutations analysis

The analysis of somatic mutations was carried out by utilizing the Mutation Annotation Format (MAF) files got from the TCGA database. To visualize the data, we created waterfall plots separately with different FDX1 groups, employing the "mafTools" package (available at: https://github.com/PoisonAlien/mafTools). A comparison was performed between the 20 most frequently mutated genes and the distribution of TMB within the FDX1-related subgroups.

2.9. Evaluation of immunological microenvironment

In TCGA, we initially employed the CIBERSORT technique for appraising immune cells infiltration. Then an evaluation process encompassed the determination of the proportional representation of 24 distinct immune cell subpopulations. To accomplish this, we relied on the "GSVA" package (v1.34.0) in the R programming language. Moreover, we incorporated the EPIC and ESTIMATE ap-proaches to contrast the extent of immune cell infiltration in TCGA, specifically within two FDX1 subgroups. We validated them in CGGA_325. Immune cell scores were calculated using each method with the aid of the R package "IOBR" (https://github.com/IOBR/IOBR).

2.10. Exploring the potential relevance of FDX1 in tumor immunotherapy

Given the remarkable efficacy of immune checkpoint blockers in human cancer treatment, we examined the expression differences and correlation between FDX1_high and FDX1_low groups with commonly used immune checkpoints in tumor immunotherapy.

2.11. Cell culture and quantitative real-time PCR (qRT-PCR)

We firstly have established stable knockdown of FDX1 in U251 and SHG44 glioma cell lines, where the shRNA lentiviral vector plasmids were purchased from Guangzhou Yunzhou Biotechnology Company. The shFDX1-1 hairpin sequence is AACAGTGGCT-GATGCCAGACAATCCATTGATGTGGGCAAGA, and the shFDX1-2 hairpin sequence is GAAGTTAGATGCAATCACTGATGAGGA-GAATGACATGCTCG. To extract total RNA from glioma cells and clinical glioma specimens, the TRIzol lysis method was employed. Subsequently, the extracted RNA was reverse-transcribed into complementary DNA (cDNA). FDX1 mRNA expression were measured by qRT-PCR using SYBR Green Master Mix. The 2-ΔΔCt method was employed to determine the levels of gene expression. The qPCR

primers utilized in this study were procured from Sangon located in Shanghai, China. The primer sequences employed for GAPDH in qPCR analysis were: the forward primer - 5'-CATTGACCTCAACTACATGGTT-3' and the reverse primer - 5'-CCATTGATGA-CAAGCTTCCC-3'. Similarly, the primers for FDX1 in qPCR assessment were the forward primer - 5'-TTGGTGCATGTGAGGGAACC-3' and the reverse primer - 5'-CAGCCCAACCGTGATCTGTC-3'.

2.12. Cell counting Kit-8 (CCK-8) assay

CCK-8 assay was utilized for evaluating cell proliferation. Each well of the 96-well plates was initially seeded with 2000 cells, followed by the introduction of 10 μL of CCK-8 reagent. After incubating the plates at 37 °C for 2 h, the absorbance was quantified at a wavelength of 450 nm. This experimental process was repeated every 24 h for a duration of 5 days.

2.13. Assessment of cell colony formation

To evaluate the glioma cells' capacity for self-growth, colony formation experiments were performed. In each well of 6-well plates, 1500 cells were seeded, and the medium was changed as necessary. Following the 12 to 14-day cell culture period, the cell colonies underwent fixation using a 4% solution of paraformaldehyde for a duration of 30 min. The colonies were then subjected to staining with 0.01% crystal violet for a duration of at least 15 min. Afterwards, the cell proliferation was measured by counting the number of colonies that were formed.

2.14. Evaluation of wound healing and transwell capabilities

To assess the wound healing and transwell potentials, we adopted the well-established methodologies as reported in prior studies
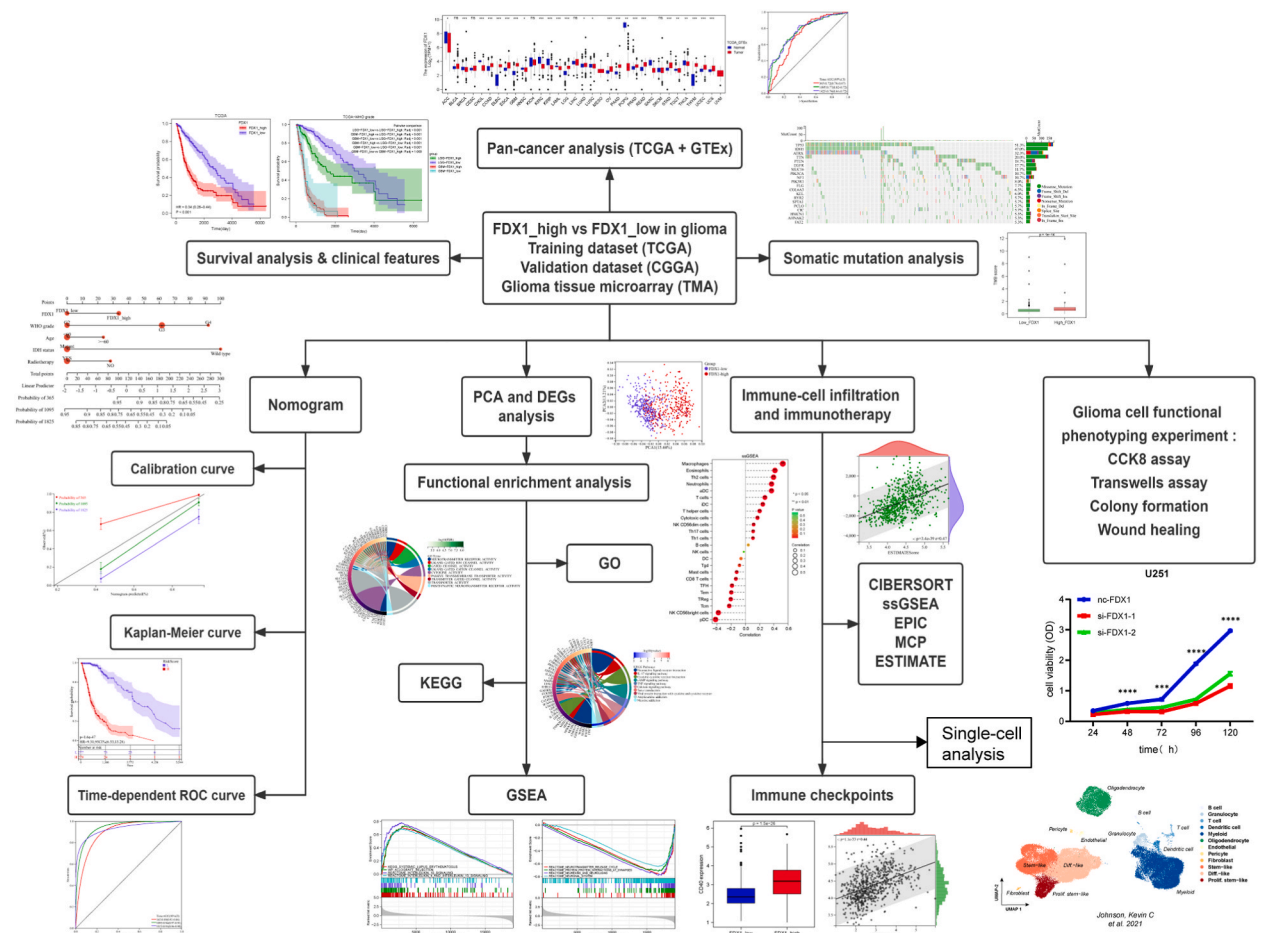
Fig. 1. Flow chart of this study. A series of bioinformatics algorithms were conducted to analyze several public databases and glioma tissue microarray. The cell experiments in vitro in this study were presented on the right side of the figure. PCA, principal component analysis; DEGs, differential expression genes; GO, gene ontology; KEGG, kyoto encyclopedia of genes and genomes; GSEA, gene set enrichment analysis.
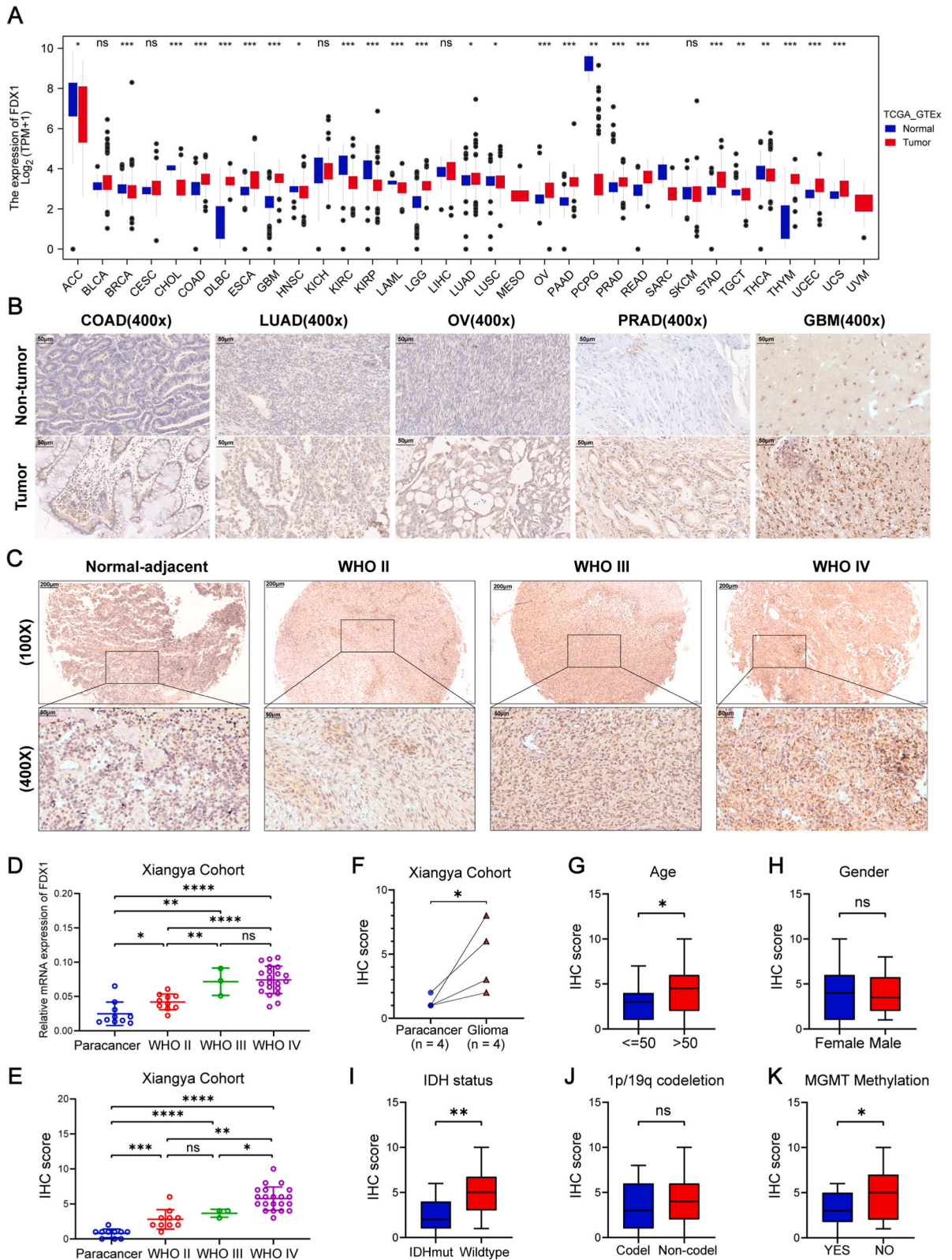
(caption on next page)

Fig. 2. **FDX1 was differentially expressed in different grades of gliomas.** (**A**) Boxplots showing the expression levels of FDX1 across tumors and normal tissues in the TCGA and GTEx cohorts. (**B**) Expression of FDX1 between tumor-adjacent tissues and COAD, LUAD, OV, PRAD, and GBM tissues by IHC. (**C-E**) Expression of FDX1 in tumor-adjacent tissue, WHO II, WHO III, and WHO IV glioma tissue by IHC and qPCR. (**F–K**) Correlation between FDX1 IHC scores with glioma grade, age, gender, IDH status, 1p/19q codeletion, and MGMT methylation calculated by one-way ANOVA and paired *t*-test methods in 44 glioma cases; *ns*, not significant; $*p < 0.05$; $**p < 0.01$; $***p < 0.005$; $****p < 0.001$.

[18,19].

2.15. EdU assays

In this experiment, cells were cultured in a 96-well plate until they reached a confluence of 70%–80%. A mixture of EdU culture medium was added to each well and incubated for 2 h. After incubation, the cells were washed with PBS and fixed with para-formaldehyde at room temperature. Glycine solution was then added and removed, followed by washing with PBS. Permeabilization buffer was added and incubated, and then the cells were washed with PBS again. Apollo staining reaction solution was added and incubated in the dark, followed by removal of the staining solution. The cells were washed with permeabilization buffer and methanol, and then washed again with PBS. Finally, DAPI fluorescent dye was added for DNA staining, and the cells were washed with PBS.

2.16. Cell cycle detection

We first performed cell cycle synchronization treatment, followed by enzymatic digestion with pancreatin, centrifugation, and resuspension of cells in PBS, repeating this process three times. Prepare pre-chilled PBS and 3 mL of anhydrous ethanol. Resuspended the cells in 1 mL of pre-chilled PBS and mixed them thoroughly. Then, we added the cell suspension dropwise to 3 mL of pre-chilled anhydrous ethanol and stored it at 4 degrees Celsi overnight or at minus 20 degrees Celsi for one week. After fixation was complete, we centrifuged the cells, discarded the supernatant, and washed the cells twice with pre-chilled PBS following the above steps. The cells were resuspended in PBS and transferred to a centrifuge tube. RNase and PI were added to the cell suspension and incubated at specific temperatures and times. Finally, a flow cytometer was used to analyze the cell cycle changes.

2.17. Statistical analysis

The statistical analysis for this study involved comparing two groups using the paired or unpaired Student's t-test. The Pearson test was employed to examine the relationship between FDX1 mRNA expression and the abundance of other genes or immune cells in independent data, utilizing one-way ANOVA to analyze multiple groups. To analyze survival rates, the researchers conducted a Kaplan-Meier survival analysis using the log-rank test. R software (version 4.0.5) or GraphPad Prism 8.0.2 was used for all statistical analyses. Significance levels were denoted as: ns, not significant; $*p < 0.05$, $**p < 0.01$, $***p < 0.005$, and $****p < 0.001$.

3. Results

3.1. Workflow of the study

The analysis process is presented in Fig. 1. To explore the association between tumors and FDX1, pan-cancer and survival analysis were performed. Additionally, a prognostic model related to FDX1 was developed using nomogram analysis. DEGs linked to FDX1 were identified, and functional enrichment analysis was carried out. Moreover, a somatic mutation analysis was undertaken to compare the FDX1_high and FDX1_low groups within the TCGA cohort. Following that, the impact of FDX1 on the infiltration of immune cells and its implications for immunotherapy were analyzed using various research techniques such as CIBERSORT, ssGSEA, EPIC, MCP, and ESTIMATE.

3.2. Correlation of FDX1 with the common tumors

We examined the association between FDX1 and various common tumors, which revealed significant differences in FDX1 gene expression across different types of tumors (Fig. 2A). These findings indicate that the involvement of FDX1 in tumor development or progression is possible. Further investigation is necessary to comprehensively comprehend the consequences of these findings and the underlying mechanisms implicated. To further investigate, we conducted protein expression analysis of FDX1 in clinical tissue samples from colorectal cancer, lung adenocarcinoma, ovarian cancer, prostate cancer, and glioma. We found that consistent with the database results, FDX1 protein was highly expressed in these tumor tissues (Fig. 2B).

3.3. FDX1 correlation with glioma's clinical characteristics

We utilized both tissue microarray and qPCR technologies. We found higher FDX1 expression in patients with higher-grade tumors, age over 50, IDH status of Wildtype, and MGMT methylation status of NO (Fig. 2C–K). We then examined several important clinical variables, including WHO grade, gender, age, IDH status, 1p/19q codeletion, radiotherapy, and chemotherapy in the TCGA cohort. A

noticeable contrast in clinical characteristics was observed between the gliomas categorized as FDX1_high and FDX1_low (Table 1; chisq test). The present study observed that the FDX1_high group exhibited a higher WHO grade and a greater proportion of "Wildtype" IDH status and non-codeletion of 1p/19q compared to the FDX1_low group in TCGA and CGGA_325 cohorts. The IDH status and 1p/ 19q codeletion served as distinct biomarkers for both glioma classification and prognostic assessment.

3.4. Survival analysis

Both the TCGA and CGGA_325 cohorts exhibited unfavorable prognoses for the FDX1_high group (Fig. 3A–D). Furthermore, in order to assess the prognostic association between FDX1 and clinical characteristics, we conducted an examination of the Kaplan-Meier survival curves. Our findings indicated that there existed a correlation between FDX1 expression and various factors including WHO grade, age, IDH status, 1p/19q codeletion, radiotherapy, and chemotherapy. These correlations suggested that FDX1 expression levels could potentially be utilized as a predictive indicator for the OS of glioma patients. The results obtained from both the TCGA and CGGA_325 cohorts indicated that the FDX1_high group exhibited a poorer prognosis, particularly in cases with WHO grade (G2, G3), age below 60, mutant IDH status, non-codel 1p/19q, and patients who received radiotherapy and chemotherapy (Fig. 3E-P, $p < 0.05$).

3.5. Validation of FDX1 as an independent prognostic factor

Univariate Cox analysis revealed that FDX1 expression level, age, WHO grade, IDH status, 1p/19q codeletion, radiotherapy, and chemotherapy were independently associated with OS in the TCGA cohort ($p < 0.01$). The multivariate Cox regression analysis identified FDX1 expression (HR 1.684; 95% CI 1.215–2.333; $p = 0.002$), WHO grade (HR 2.807; 95% CI 1.744–4.508; $p < 0.001$ and HR 4.612; 95% CI 2.649–8.049; $p < 0.001$), age (HR 1.442; 95% CI 1.036–2.007; $p = 0.030$), IDH status (HR 4.878; 95% CI 3.171–7.503; $p < 0.001$), and radiotherapy (HR 0.611; 95% CI 0.382–0.976; $p = 0.039$) as key factors for prognostic modeling in the TCGA cohort (Fig. 4A). In addition, a nomogram was created to assess the duration of survival for patients with glioma over the course of 365, 1095, and 1825 days (Fig. 4B). At 365, 1095, and 1825 days, the calibration plot demonstrated a favorable association linking the projected and real OS values among glioma patients (Fig. 4C). Following that, the TCGA cohort exhibited that the RiskScore-H group had an unfavorable prognosis in comparison to the RiskScore-L group (Fig. 4D). Moreover, the analysis of time-dependent receiver operating characteristic (ROC) curves displayed desirable sensitivity and specificity, with AUCs of 0.89, 0.94, and 0.93 at 365, 1095, and 1825 days (Fig. 4E).

The predictive power of FDX1 in prognosis was verified by validating it in the CGGA_325 cohort. A prognostic model was developed

Table 1
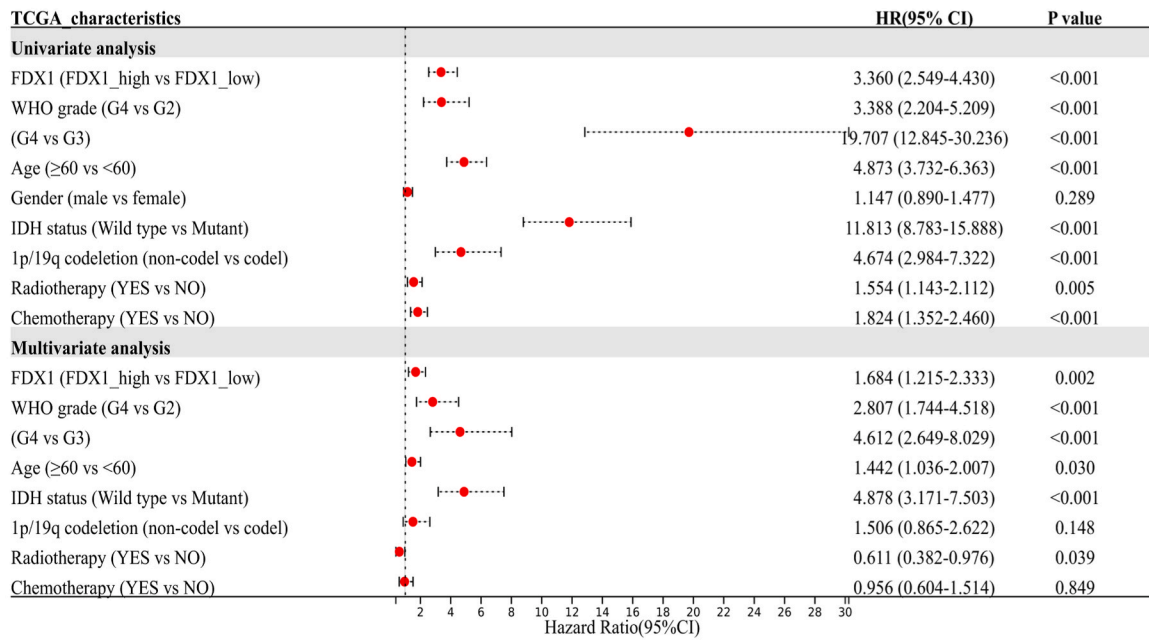Baseline characteristics of the patients with FDX1 expression in cohorts.

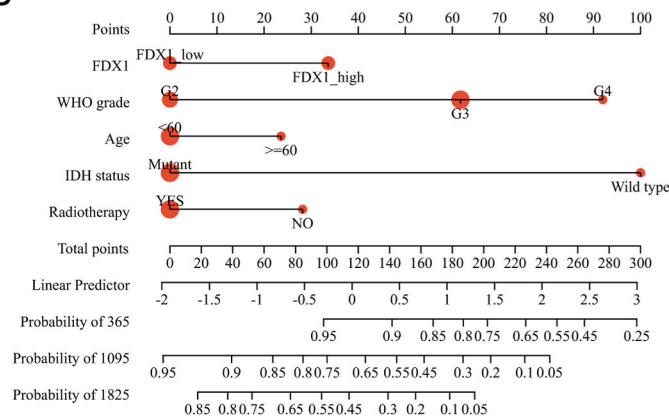| Variables	TCGA cohort				CGGA_325 cohort			
	FDX1_high(n = 341)	FDX1_low(n = 341)	p	method	FDX1_high(n = 163)	FDX1_low(n = 162)	p	method
Grade, n (%)	-	–	<0.001	Chisq. test	–	–	0.002	Chisq. test
G2	69 (11.1%)	151 (24.4%)	–	–	37 (11.5%)	66 (20.6%)	–	–
G3	111 (17.9%)	126 (20.3%)	–	–	44 (13.7%)	35 (10.9%)	–	–
G4	136 (21.9%)	27 (4.4%)	–	–	81 (25.2%)	58 (18.1%)	–	–
Age, n (%)	-	–	<0.001	Chisq. test	–	–	0.474	Chisq. test
<60	242 (35.6%)	282 (41.5%)	–	–	144 (44.3%)	148 (45.5%)	–	–
≥60	99 (14.6%)	57 (8.4%)	–	–	19 (5.8%)	14 (4.3%)	–	–
IDH status, n (%)	-	–	<0.001	Chisq. test	–	–	0.001	Chisq. test
Mutant	151 (22.5%)	278 (41.5%)	–	–	73 (22.5%)	102 (31.5%)	–	–
Wild type	182 (27.2%)	59 (8.8%)	–	–	90 (27.8%)	59 (18.2%)	–	–
1p/19q codeletion, n (%)	-	–	<0.001	Chisq. test	–	–	<0.001	Chisq. test
codel	25 (3.7%)	145 (21.5%)	–	–	14 (4.4%)	53 (16.7%)	–	–
non-codel	310 (46%)	194 (28.8%)	–	–	145 (45.7%)	105 (33.1%)	–	–
Gender, n (%)	-	–	0.929	Chisq. test	–	–	0.699	Chisq. test
female	147 (21.6%)	144 (21.2%)	–	–	59 (18.2%)	63 (19.4%)	–	–
male	194 (28.5%)	195 (28.7%)	–	–	104 (32%)	99 (30.5%)	–	–
Radiotherapy, n (%)	-	–	<0.001	Chisq. test	–	–	0.811	Chisq. test
NO	100 (15.2%)	150 (22.8%)	–	–	31 (10%)	35 (11.3%)	–	–
YES	230 (35%)	178 (27.1%)	–	–	121 (39%)	123 (39.7%)	–	–
Chemotherapy, n (%)	-	–	<0.001	Chisq. test	–	–	0.209	Chisq. test
NO	111 (16.3%)	165 (24.3%)	–	–	49 (16.1%)	62 (20.4%)	–	–
YES	229 (33.7%)	175 (25.7%)	–	–	101 (33.2%)	92 (30.3%)	–	–
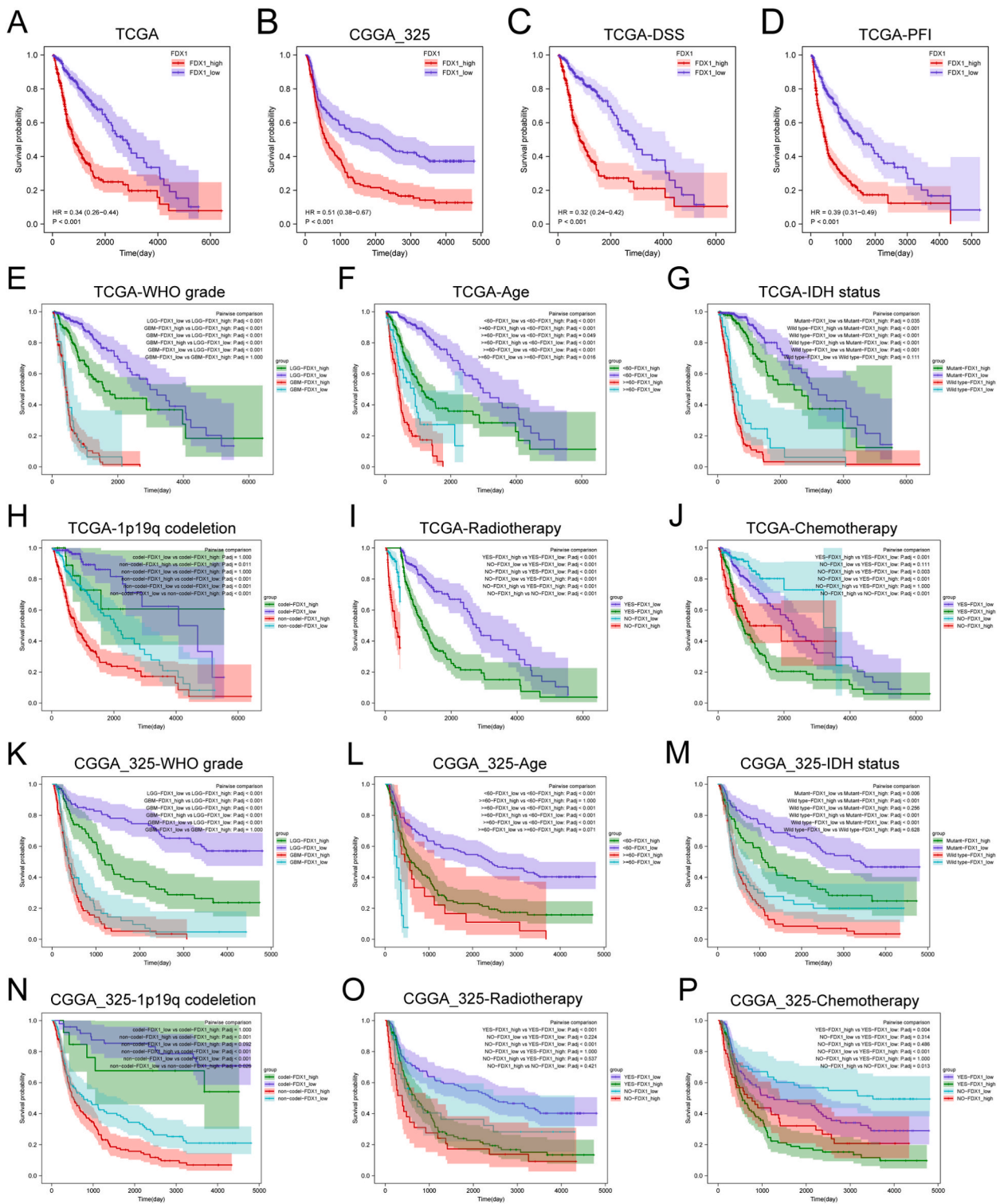
Fig. 3. Survival analysis in the FDX1_high and FDX1_low groups and several vital clinical subgroups. (**A-B**) OS in TCGA and CGGA_325. (**C-D**) DSS and PFI in TCGA. Clinical subgroups-related overall survival analysis in TCGA and CGGA_325.(**E, K**) WHO grade. (**F, L**) Age. (G, M) IDH status. (**H, N**) 1p19q codeletion. (**I, O**) Radiotherapy. (**J, P**) Chemotherapy.

A

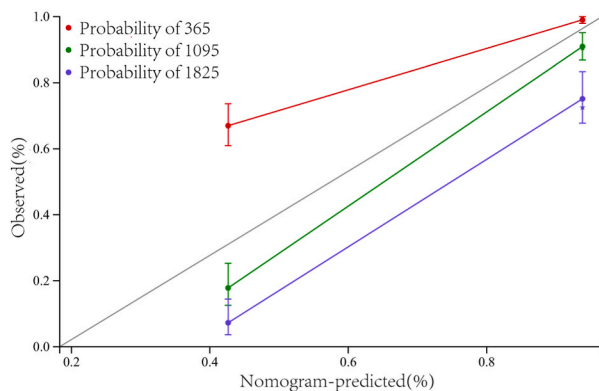| TCGA_characteristics		HR(95% CI)	P value
Univariate analysis			
FDX1 (FDX1_high vs FDX1_low)		3.360 (2.549-4.430)	<0.001
WHO grade (G4 vs G2)		3.388 (2.204-5.209)	<0.001
(G4 vs G3)		19.707 (12.845-30.236)	<0.001
Age (≥60 vs <60)		4.873 (3.732-6.363)	<0.001
Gender (male vs female)		1.147 (0.890-1.477)	0.289
IDH status (Wild type vs Mutant)		11.813 (8.783-15.888)	<0.001
1p/19q codeletion (non-codel vs codel)		4.674 (2.984-7.322)	<0.001
Radiotherapy (YES vs NO)		1.554 (1.143-2.112)	0.005
Chemotherapy (YES vs NO)		1.824 (1.352-2.460)	<0.001
Multivariate analysis			
FDX1 (FDX1_high vs FDX1_low)		1.684 (1.215-2.333)	0.002
WHO grade (G4 vs G2)		2.807 (1.744-4.518)	<0.001
(G4 vs G3)		4.612 (2.649-8.029)	<0.001
Age (≥60 vs <60)		1.442 (1.036-2.007)	0.030
IDH status (Wild type vs Mutant)		4.878 (3.171-7.503)	<0.001
1p/19q codeletion (non-codel vs codel)		1.506 (0.865-2.622)	0.148
Radiotherapy (YES vs NO)		0.611 (0.382-0.976)	0.039
Chemotherapy (YES vs NO)		0.956 (0.604-1.514)	0.849

Hazard Ratio(95%CI)
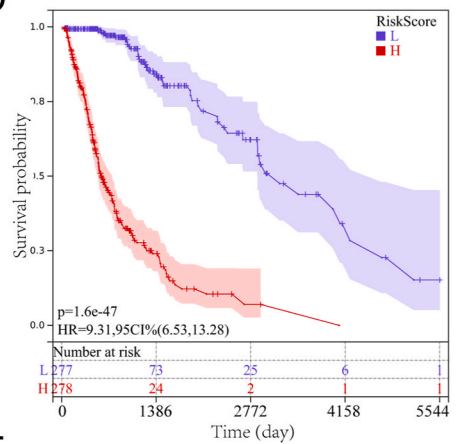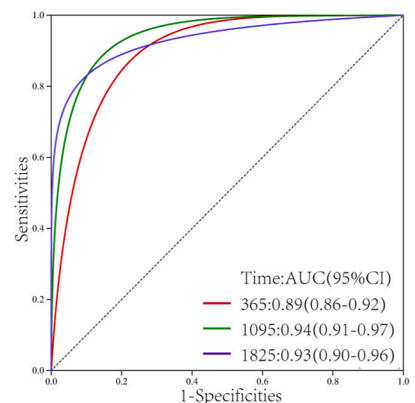
(caption on next page)

Fig. 4. The FDX1 expression predicts prognosis in glioma patients in the TCGA cohort. (**A**) Univariate and multivariate analysis based on FDX1 expression and clinical characteristics in the TCGA cohort. (**B**) Nomogram predicts 1-, 3-, and 5-year overall survival in glioma patients in the TCGA cohort. (**C**) Calibration plot of the nomogram. (**D**) Kaplan-Meier survival curves by riskscore level for glioma patients in the TCGA cohort. (**E**) The time-dependent ROC of the nomogram predicts 1-, 3-, and 5-year overall survival. HR refers to hazard ratio; CI refers to the confidence interval.

that included FDX1 expression (HR 1.445; 95% CI 1.073–1.945; $p = 0.015$), along with WHO grade (HR 4.007; 95% CI 2.518–6.376; $p < 0.001$ and HR 7.578; 95% CI 4.744–12.105; $p < 0.001$), age (HR 1.537; 95% CI 1.012–2.335; $p = 0.044$), 1p/19q codeletion (HR 3.105; 95% CI 1.807–5.335; $p < 0.001$), and chemotherapy (HR 0.660; 95% CI 0.474–0.918; $p = 0.014$) (Fig. 5A). The effectiveness of the FDX1-related prognostic model in predicting patient outcomes in the CGGA_325 cohort was evaluated using a nomogram and calibration chart (Fig. 5B–C). The survival and ROC curves showed that the model accurately predicted patient prognosis with high AUC values of 0.80, 0.88, and 0.91 at 365, 1095, and 1825 days (Fig. 5D–E).

3.6. Differential analysis and signaling pathways based on FDX1 level in glioma

To assess the differential analysis and signaling pathways based on FDX1 level in glioma, we conducted a principal component analysis (PCA), revealing a great distinction in the distribution patterns of the subgroups (Fig. 6A). Subsequently, we applied the DEG analysis between the subgroups in TCGA. A count of 233 differentially expressed genes (DEGs) was acquired, with 152 exhibiting upregulation and 81 displaying downregulation (FDR <0.05, |log2 FC| > 2.0, and $p < 0.05$) (Fig. 6B). We identified the top 10 upregulated genes and 5 downregulated genes among the various genes. This was done by determining their |log2 FC| values. The GO analysis revealed a focus on signal transduction functions, such as cell signaling and transport activity (Fig. 6C–E). The KEGG enrichment analysis revealed tumor-associated biological processes, such as the tumor necrosis factor signaling pathway, immune-related processes such as the interleukin-17 signaling pathway, cytokine-cytokine receptor interaction, and viral protein interaction with cytokine and cytokine receptor (Fig. 6F). The results of the GSEA showed that the top 4 upregulated terms were closely related to immune biological processes, such as systemic lupus erythematosus, allograft rejection, interleukin-4 and interleukin-13 signaling, and interleukin-10 signaling, while the top 4 downregulated terms were associated with neuronal function processes, including neurotransmitter release cycle, protein-protein interactions at synapses, neurexins, and neuroligins, and the neuronal system (Fig. 6G–H). The results implied that FDX1 could potentially act as an indicator of the immune response within gliomas.

3.7. Somatic mutations analysis

Studies have shown that tumor-specific mutations can result in neoantigens, activate immune recognition, and eventually cause tumor cell death [20,21]. To assess the disparities in somatic mutation frequencies between the two FDX1-related groups in glioma, the average expression level of FDX1 was evaluated. The 20 most frequently mutated genes in both groups were identified (Fig. 7A–B). Glioma development and progression are significantly linked to the occurrence of eight frequently mutated genes including TP53, TNN, PTEN, EGFR, ATRX, PIK3CA, IDH1, and CIC [22–24]. Notably, the FDX1_high group exhibited a higher mutation ratio of malignancy-related genes such as EGFR and TTN. The mutation proportion of tumor suppressor genes such as IDH1 and CIC were higher in the FDX1_low group (Fig. 7C). Furthermore, the FDX1_high group exhibited a higher TMB (Fig. 7D), indicating that the genome of these samples may be more unstable, and FDX1 may play a crucial role in tumorigenesis.
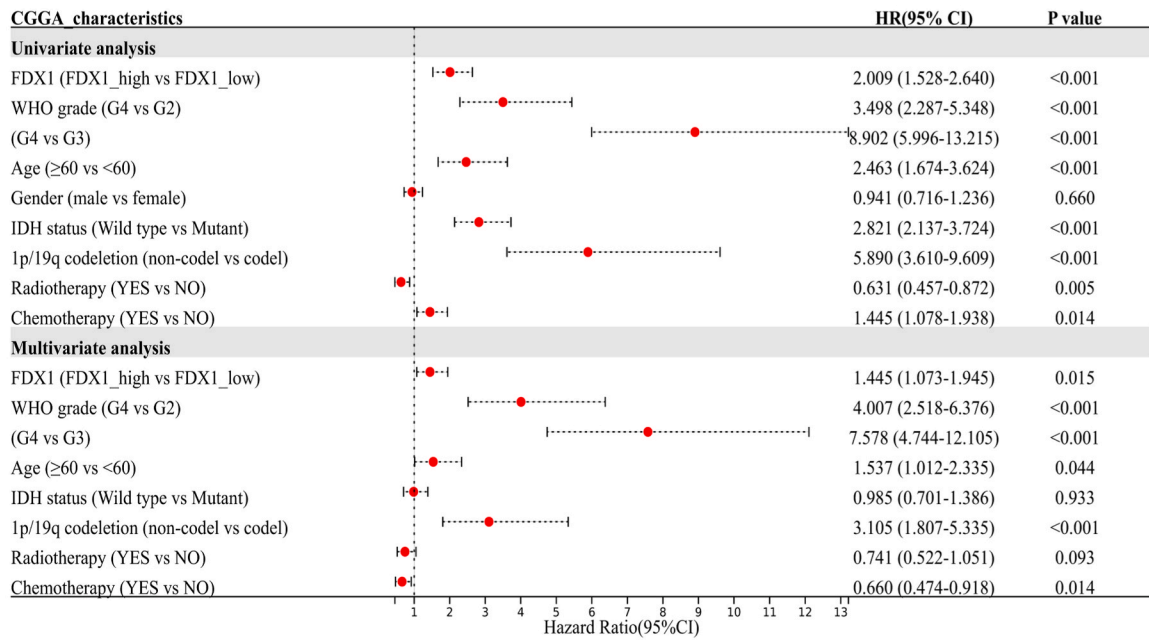
3.8. Evaluation of immunological microenvironment

We first utilized the CIBERSORT approach to validate the correlation linking FDX1 expression and immune constituents. Utilizing this approach, immune cell profiles were constructed across 32 different tumor types, encompassing a total of 28 distinct cell types (Fig. 8A). In GBM, CD56 bright natural killer (NK) cells positively correlated with FDX1 expression, while CD56 dim NK cells correlated negatively. In LGG, most immune cells positively correlated with FDX1 expression, except for monocytes and effector memory CD4$^+$ T cells. The ssGSEA analysis revealed that 21 types of tumor-infiltrating immune cells (TICs) were positively related to FDX1 expression (Fig. 8B). Twelve TICs were positively related, including macrophages, eosinophils, Th2 cells, neutrophils, activated Dendritic cells (aDC), T cells, immature Dendritic cells (iDC), T helper cells, cytotoxic cells, NK CD56dim cells, Th17 cells, and Th 1 cells. Nine TICs were negatively correlated with FDX1 expression, including gamma delta T cells, mast cells, CD8$^+$ T cells, follicular helper T cells (TFH cells), effector memory T cells (TEM cells), regulatory T cells (Treg cells), central memory T cells (TCM cells), NK CD56bright cells, and plasmacytoid Dendritic cells (pDC). The findings presented in this study demonstrated the substantial influence of FDX1 expression on immune function within the tumor microenvironment. Analysis using EPIC demonstrated a clear association between FDX1 expression levels and multiple cell populations, such as T cells, neutrophils, macrophages, and cancer-associated fibroblasts (CAFs), in both TCGA and CGGA_325 datasets (Fig. 8C). The FDX1 expression was significantly related to higher ESTIMATE-related scores (StromalScore, ImmuneScore, and ESTIMATEScore) (p < 0.0001) in the FDX1_high group of patients (Pearson's correlation coefficient test, in TCGA, |r| > 0.4; in CGGA_325, |r| > 0.3, Fig. 8D).
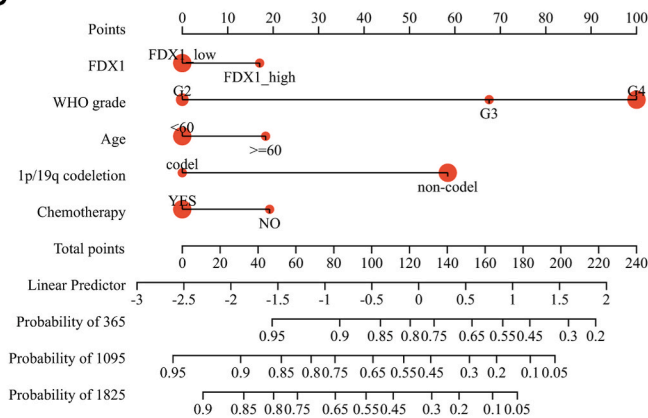
3.9. Single-cell RNA-seq bioinformatics analysis

In this study, sequencing data from 11 glioma patients were analyzed. Using unsupervised clustering analysis, a comprehensive
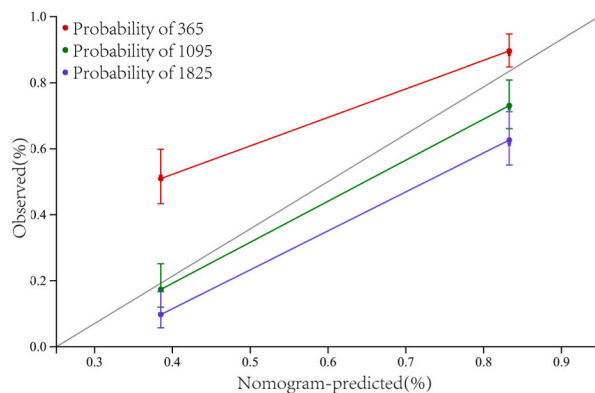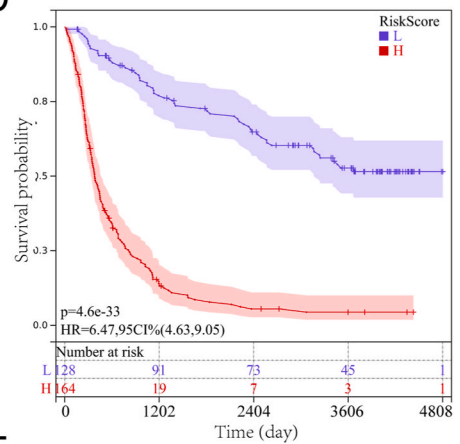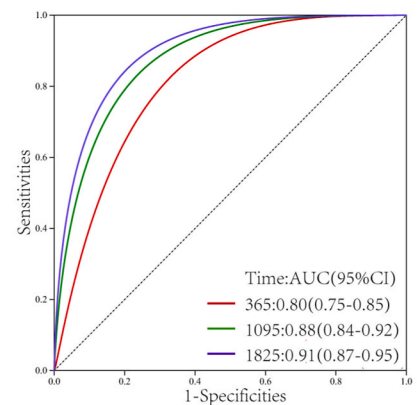
A

CGGA_characteristics		HR(95% CI)	P value
Univariate analysis			
FDX1 (FDX1_high vs FDX1_low)		2.009 (1.528-2.640)	<0.001
WHO grade (G4 vs G2)		3.498 (2.287-5.348)	<0.001
(G4 vs G3)		8.902 (5.996-13.215)	<0.001
Age (≥60 vs <60)		2.463 (1.674-3.624)	<0.001
Gender (male vs female)		0.941 (0.716-1.236)	0.660
IDH status (Wild type vs Mutant)		2.821 (2.137-3.724)	<0.001
1p/19q codeletion (non-codel vs codel)		5.890 (3.610-9.609)	<0.001
Radiotherapy (YES vs NO)		0.631 (0.457-0.872)	0.005
Chemotherapy (YES vs NO)		1.445 (1.078-1.938)	0.014
Multivariate analysis			
FDX1 (FDX1_high vs FDX1_low)		1.445 (1.073-1.945)	0.015
WHO grade (G4 vs G2)		4.007 (2.518-6.376)	<0.001
(G4 vs G3)		7.578 (4.744-12.105)	<0.001
Age (≥60 vs <60)		1.537 (1.012-2.335)	0.044
IDH status (Wild type vs Mutant)		0.985 (0.701-1.386)	0.933
1p/19q codeletion (non-codel vs codel)		3.105 (1.807-5.335)	<0.001
Radiotherapy (YES vs NO)		0.741 (0.522-1.051)	0.093
Chemotherapy (YES vs NO)		0.660 (0.474-0.918)	0.014

Hazard Ratio(95%CI)

(caption on next page)

Fig. 5. The FDX1 expression predicts poor prognosis in glioma patients in the CGGA_325 cohort. (**A**) Univariate and multivariate analyses based on FDX1 expression and clinical characteristics in the CGGA_325 cohort. (**B**) Nomogram predicting 1-, 3-, and 5-year overall survival for glioma patients in the CGGA_325 cohort. (**C**) The calibration plot of the nomogram. (**D**) Kaplan Meier survival curve of glioma patients in the CGGA_325 cohort with riskscore level. (**E**) The time-dependent ROC of the nomogram predicts 1-, 3-, and 5-year overall survival. HR refers to hazard ratio; CI refers to the confidence interval.

investigation was conducted on individual cells, resulting in the identification of 12 distinct clusters. These clusters were determined through the evaluation of marker gene expression, enabling the identification of separate populations comprising glial cells, immune cells, stromal cells, and malignant cells (Fig. 8E). The results showed that FDX1 could express in all 12 types of cells (Fig. 8F). And the expression of FDX1 was upregulated mainly in the Prolif.stem-like, Diff.-like, and Dendritic cells in glioma samples (Fig. 8G).

3.10. FDX1 correlated with immune checkpoint therapy in glioma

Glioma, particularly glioblastoma, is a type of immunosuppressive brain cancer. Immune checkpoint therapy has shown promising results in multiple cancers and significant advances have been made in the preclinical research of glioma. Hence, the expression difference and correlation between FDX1 and immune checkpoint markers were investigated. We conducted an analysis on the TCGA cohort and observed that patients categorized within the FDX1_high group exhibited elevated levels of immune checkpoint markers (PD-1, PD-L1, CD40, CD80, and CD86). Indeed, the relationship between tumor immunity and FDX1 has been extensively investigated in various malignant tumors [25–27]. Additionally, a significant and noteworthy correlation has been observed between the expression of FDX1 and the immune checkpoint markers mentioned above (Pearson test, for PD-1, $r = 0.43$; for PD-L1, $r = 0.48$; for CD40, $r = 0.44$; for CD80, $r = 0.54$; for CD86, $r = 0.54$, Fig. 9A–E). The FDX1_high group in the CGGA_325 cohort demonstrated high expression of immune checkpoint markers, which exhibited a positive correlation with FDX1 expression (Pearson test, for PD-1, $r = 0.20$; for PD-L1, $r = 0.33$; for CD40, $r = 0.28$; for CD80, $r = 0.23$; for CD86, $r = 0.36$, Fig. 9F–J). The findings provided a potential strategy for immunotherapy in glioma patients.

3.11. Suppression of FDX1 inhibited the proliferation, migration, invasion, and G2-M phase transition in glioma cells

We first evaluated its biological functions in U251 and SHG44 cell lines derived from glioma. FDX1 gene knockdown was achieved via two shRNA lentiviral vector plasmids, targeting FDX1 (shFDX1-1 and shFDX1-2). As demonstrated by the qRT-PCR results, transfection with either shFDX1-1 or shFDX1-2 significantly downregulated FDX1 expression (Fig. 10A). The CCK-8 analysis revealed that the growth rate of U251 and SHG44 cells was hindered in the shFDX1 experimental groups (Fig. 10B). Furthermore, knockdown of FDX1 in both cell lines caused colonies generated and the proportion of EdU positive cells to decrease(Fig. 10C–F). Wound healing and Transwell assays presented that the glioma cells' migrating and invading were weakened after FDX1 gene knockdown (Fig. 11A–D). Flow cytometry detected cell cycle arrest at G2-M phase resulting from FDX1 knockdown (Fig. 11E–F). The findings as a whole indicated that FDX1 may hold a significant position in the metastatic phenotypes of gliomas.
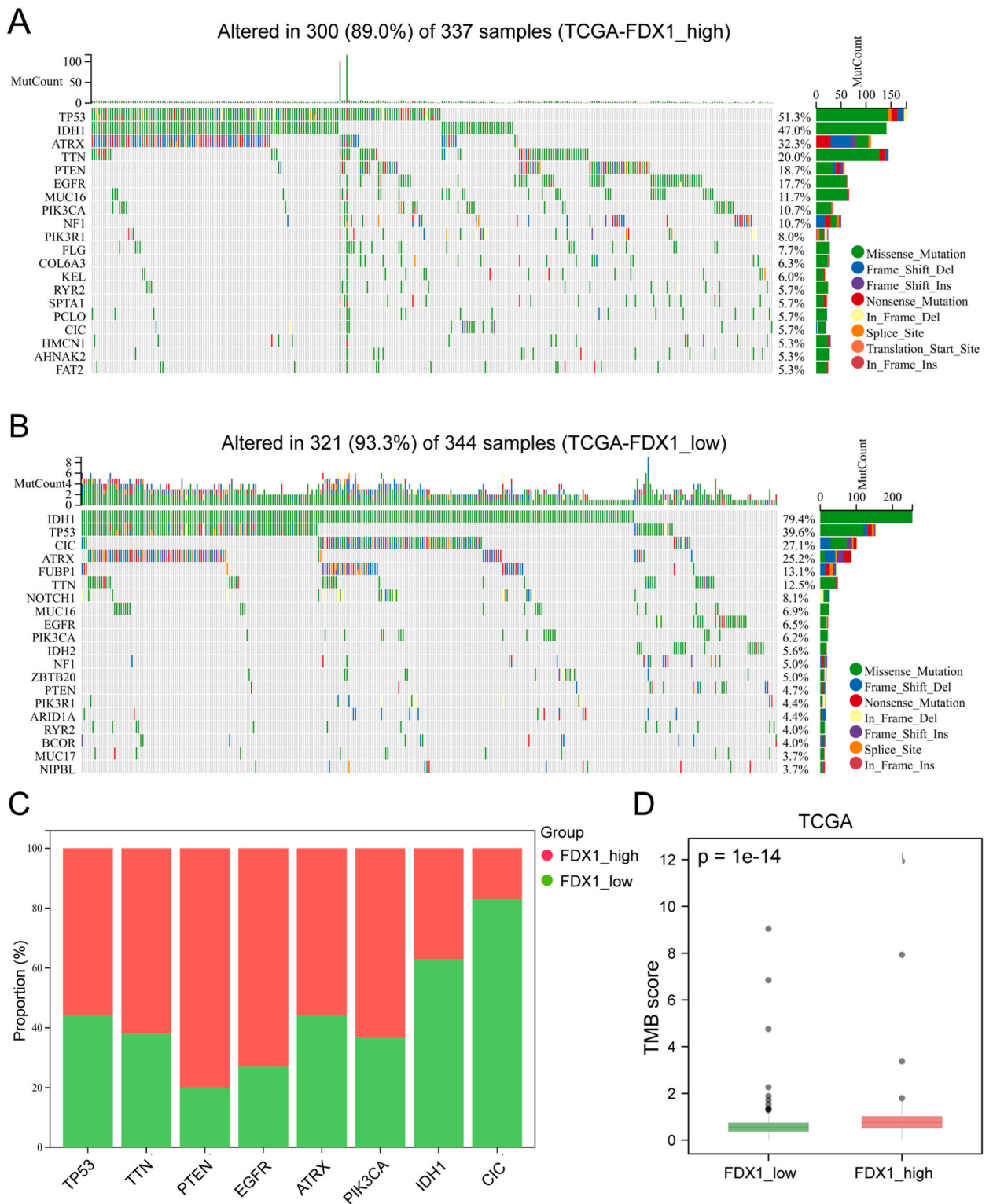
4. Discussion

Gliomas, the most common and fatal brain tumors, have previously shown a strong link to FDX1 and cuproptosis [11]. The objective of this investigation was to examine the manifestation of FDX1 in glioma specimens and its association with the malignancy of glioma. FDX1 was identified as an autonomous prognostic determinant for glioma by conducting both univariate and multivariate Cox analyses. The GSEA revealed that several immune-related pathways were upregulated, while some neural function-related processes were downregulated, with the FDX1_high group exhibiting increased immune cell infiltration.

FDX1 participated in the transfer of electrons from NADPH to cytochrome P450 in the mitochondria through the action of ferredoxin reductase. Moreover, it was essential for several metabolic pathways, including the metabolism of steroids, vitamin D, and bile acids, as well as being implicated in the occurrence of cuproptosis. However, there have been no studies on FDX1 in glioma. Copper-dependent anticancer agents, such as DSF/Cu, Cu(DDC)2, quinoline, and compounds from the dithiocarbamate family, could induce cancer cell apoptosis and play a non-toxic role in anti-cancer effects [28,29]. In glioma patients, the expression of FDX1 appeared to be linked to clinical characteristics and poor prognosis in public databases, as determined using tissue microarray from the Xiangya cohort. Additionally, this effect was observed in both short-term and long-term survival, with FDX1 expression determined as an autonomous prognostic determinant in the Univariate Cox regression analysis, besides other clinical features. Multivariate Cox analysis showed that FDX1, along with other clinical variables like WHO grade, IDH status, and 1p/19q codeletion, exhibited prognostic significance in glioma patients. Therefore, FDX1 could potentially function as an innovative biomarker, offering insights into the connection between cuproptosis, glioma development, and patient survival outcome.

In this study, functional analyses (GO analysis, KEGG analysis, and GSEA analysis) indicated that FDX1 might regulate the tumor immune response through IL-4, IL-13, and IL-10 signaling. Research findings have shown that the inhibition of IL-4 leads to an increase in the synthesis of IL-12 by MregDC1s that bear tumor antigens, thereby leading to the expansion of effector T cells [30]. Moreover, IL-4 and IL-13 Pseudomonas exotoxins have been utilized in the management of brain tumors [31]. IL-10 suppressed the responses of macrophages and pro-inflammatory Th17 T cells by inhibiting IL-6 and IL-12/23 [31]. By regulating inflammation, IL-10 has been shown to be involved in antitumor immunity [32,33]. The study suggested that FDX1 may participate in regulating the tumor

Fig. 6. PCA analysis and enrichment analysis. (**A**) PCA plot analysis in FDX1_high and FDX1_low groups in the TCGA cohort. (**B**) Volcano plot for differentially expressed genes. (**C-E**) Enrichment analysis of GO-BP, GO-CC, GO-MF. (**F**) Enrichment analysis of KEGG. (**G-H**) The top 4 upregulated and downregulated pathways of GSEA analysis.

Fig. 7. Somatic mutation analyses between FDX1_high and FDX1_low groups in the TCGA cohort. (**A**) and (**B**) Waterfall plot respectively shows the mutation distribution of the top 20 most frequently mutated genes in FDX1_high and FDX1_low groups. (**C**) The proportion of several vital cancer-associated mutated genes between FDX1-high and FDX1_low group in the TCGA cohort. (**D**) Correlation between TMB and the expression of FDX1 in the TCGA cohort.
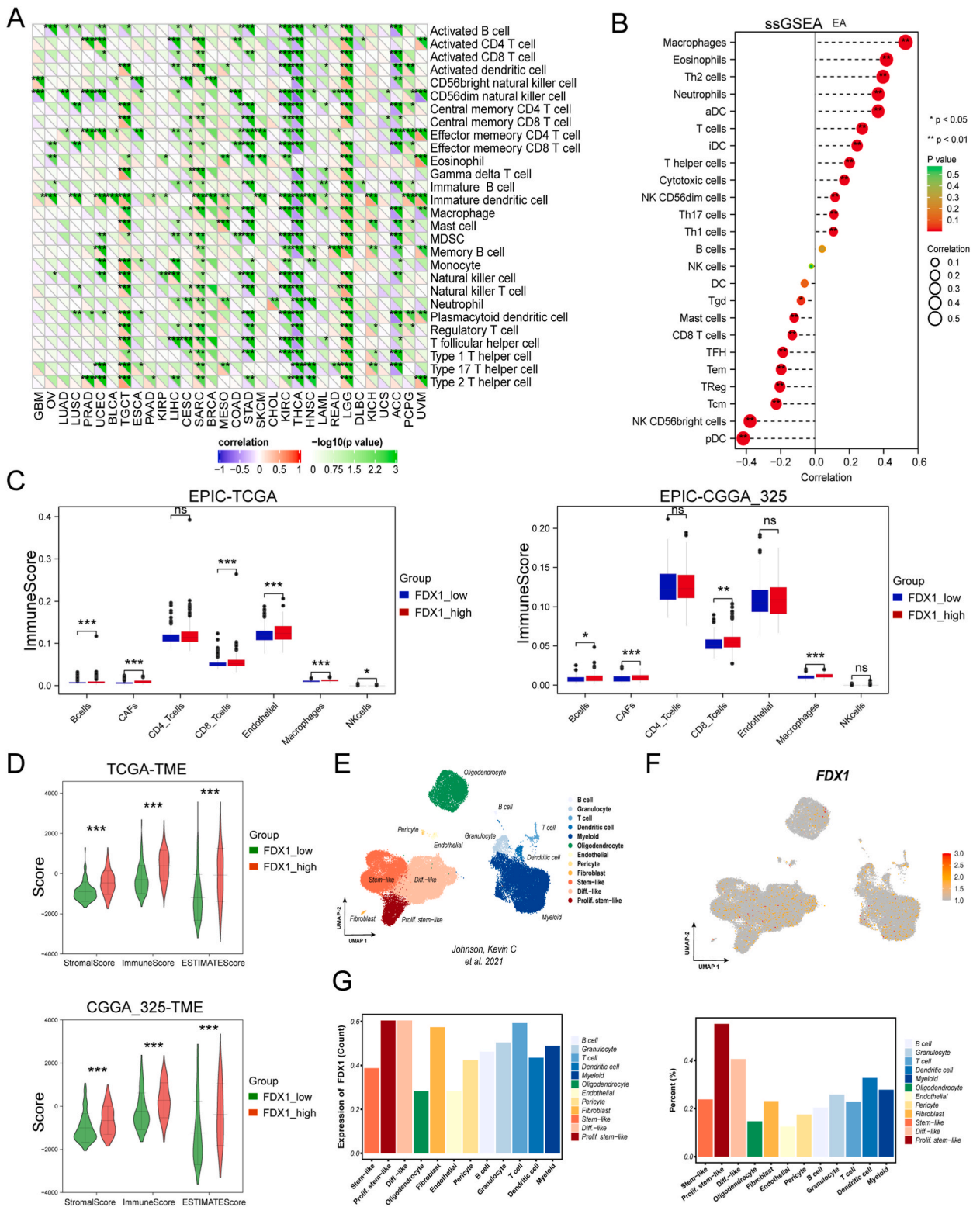
(caption on next page)

Fig. 8. Correlation analysis between FDX1 expression and tumor immune microenvironment. (**A**) Pan-cancer correlation analysis of the FDX1 expression with 28 immune cells in TCGA by CIBERSORT. (|Pearson r| > 0.2). (**B**) The ssGSEA analysis for the FDX1 expression with 24 types of immune cells in the TCGA cohort. (**C**) The EPIC analysis for the FDX1 expression in the TCGA and CCGA_325 cohorts. (**D**) Distribution of ImmuneScore, StromalScore, and ESTIMATEScore between the FDX1_high and FDX1_low group in the TCGA and CCGA_325 cohorts. (**E**) Cell markers for clusters' annotation. (**F-G**) The FDX1 expression in tissues extracted from the Johnson, Kevin C et al. ns, not significant; *$p < 0.05$; **$p < 0.01$; ***$p < 0.001$.

microenvironment and have potential in complementing glioma typing. The investigation on the association between FDX1 expression and the tumor immune microenvironment demonstrated that FDX1 enhanced the infiltration of various immune cells and non-tumor cells. However, single-cell analysis showed that FDX1 was expressed in all cell populations, mainly in the Prolif.stem-like, Diff.-like, and Dendritic cells. Further exploration of the interplay and communication between immune infiltrating cells and tumor cells via FDX1 alterations could offer novel insights into effective treatment strategies, ultimately enhancing the standard of glioma care.

Shifting the tumor microenvironment from being tumor-friendly to tumor-suppressive has been shown to be a promising strategy for improving tumor therapy [34]. In the case of gliomas, unique brain immune mechanisms lead to the formation of specific microenvironments [35]. In these microenvironments, several peripheral immune components, including myeloid-derived suppressor cells (MDSCs), macrophages, natural killer cells (NK cells), neutrophils, CD4$^+$ helper T cells (Th), regulatory T (Treg) cells, and CD8$^+$ toxic T lymphocytes (CTLs), were present at low levels compared to other tumors [36,37]. Despite the potential of immunotherapy in treating gliomas, preclinical models have shown that patients rarely benefit due to poor responses and high heterogeneity [35,38]. Therefore, it is crucial to identify innovative therapeutic targets and reduce heterogeneity through a comprehensive analysis of multi-layered data.

Moreover, there is growing evidence to suggest that neoantigens generated by tumor-specific mutations can trigger immune recognition and eliminate cancer cells, highlighting the potential for modifying specific genes to alter the tumor microenvironment [39,40]. Through the utilization of transcriptomic RNA-seq and somatic mutation data, the amalgamation of bioinformatics analyses depicted a noteworthy association between heightened expression of FDX1 and amplified mutations in genes with unfavorable prognosis, for instance TP53, while decreased mutations were observed in favorable prognostic genes like IDH1. Furthermore, the FDX1_high group exhibited a higher mutation rate, indicating that increased FDX1 expression may impede the expression of tumor-specific antigens and promote tumor progression.

Checkpoint inhibitors have shown clinical success in several solid tumors, increasing interest in immune-specific treatments for gliomas. To explore the correlation of FDX1 with different immunity checkpoints, the expression of FDX1 was analyzed with immunity checkpoint markers [35,41,42]. According to the findings, individuals belonging to the FDX1_high group displayed increased levels of immunity checkpoint markers expression. This poor prognosis may be due to tumor immunosuppression and highlights the potential of cuproptosis in immunotherapy. The results of in vitro experiments confirmed that FDX1 positively correlates with the proliferation, migration, invasion ability and G2-M phase transition of glioma cells.

Our research emphasizes that FDX1 had a significant impact on clinical outcomes and malignant phenotype s in individuals with glioma. Nevertheless, our study remains highly limited, and further research is needed to determine if the novel cell death pathways are associated with the intrinsic functional mechanisms of FDX1 in the malignant advancement of gliomas, such as copper-induced cell death, and what role cellular immune responses play.

Funding

Ethical approval statement

This study was reviewed and approved by [The Human Ethics Committee of Xiangya Hospital], with the approval number: [202303044]. All patients provided informed consent to participate in the study.

Data availability statement

The data used for bioinformatics analysis in this study are all from public databases, and the data sources have been explained in the paper. The datasets for this study can be found in TCGA (http://cancergenome.nih.gov/), CGGA(http://www.cgga.org.cn/), and GTEx (http://commonfund.nih.gov/GTEx/).

CRediT authorship contribution statement

Dongcheng Xie: Writing – review & editing, Writing – original draft, Software, Resources, Project administration, Methodology, Formal analysis, Data curation, Conceptualization. **Hailong Huang:** Writing – review & editing, Software, Resources, Methodology, Formal analysis, Data curation. **Youwei Guo:** Writing – review & editing, Software, Resources, Project administration, Data curation.
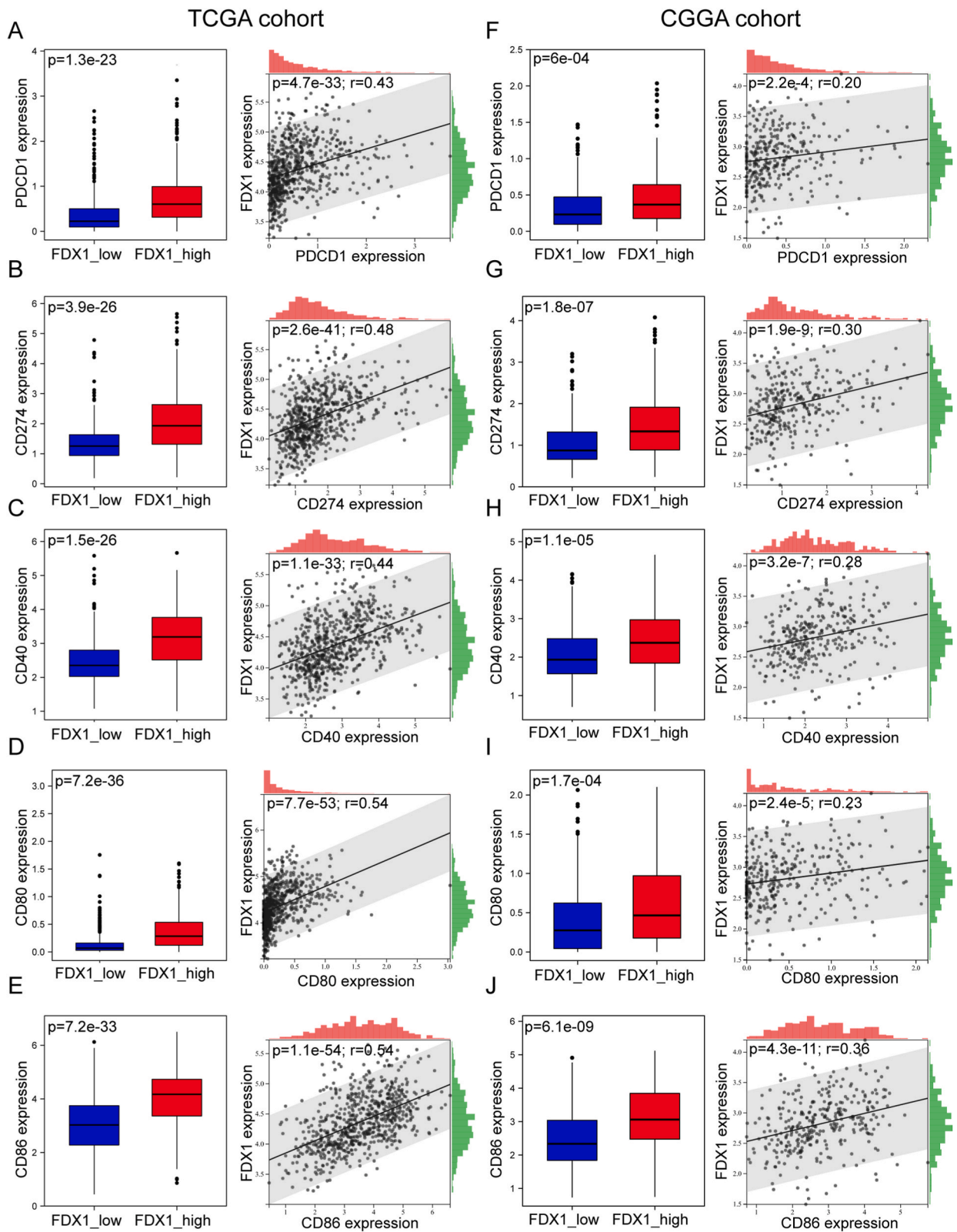
Fig. 9. The expression difference and correlation between several vital immune checkpoints and FDX1 expression level in the TCGA and CGGA_325 cohorts. (**A, F**) PDCD1, (**B, G**) CD274, (**C, H**) CD40, (**D, I**) CD80, (**E, J**) CD86.
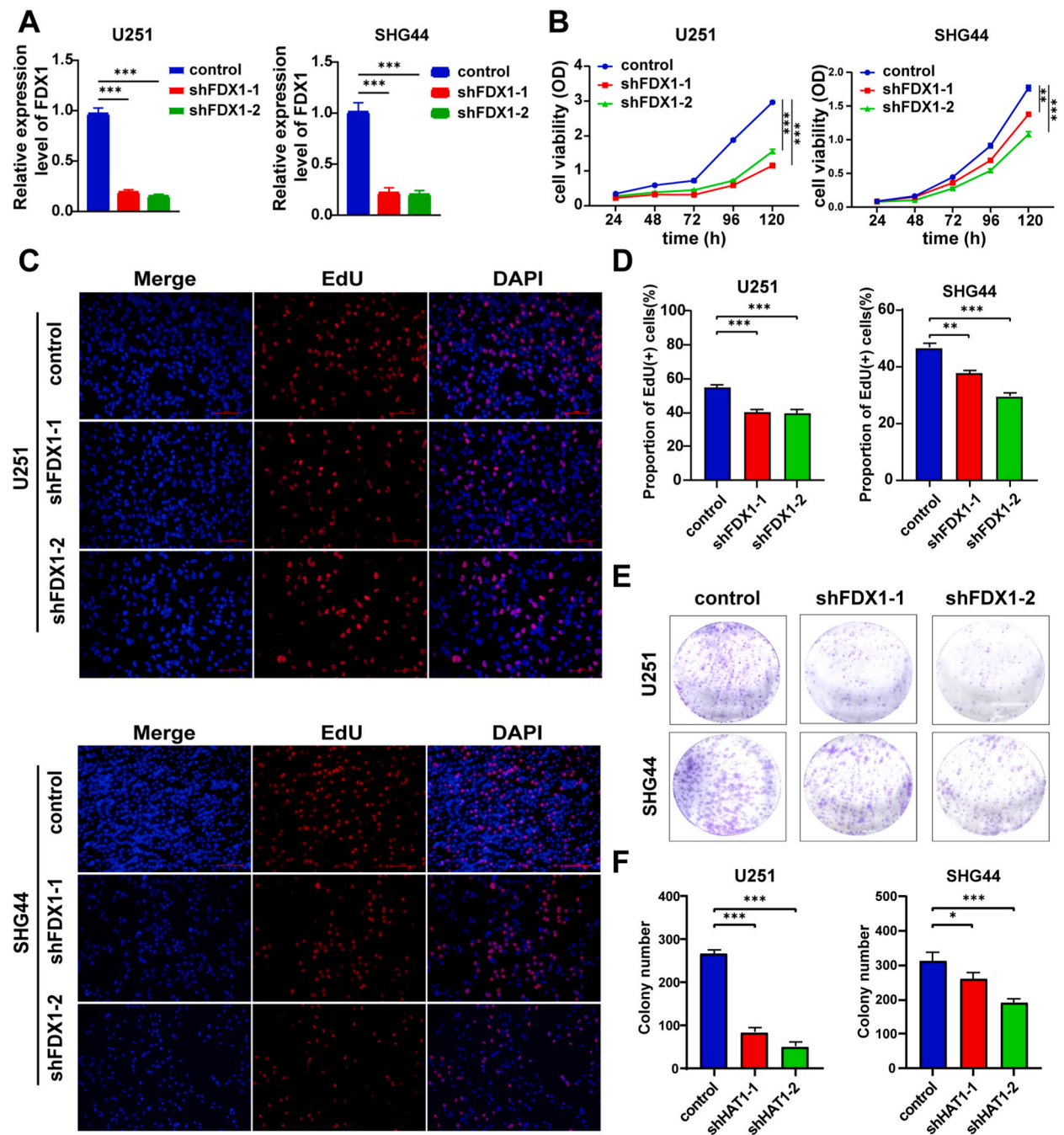
Fig. 10. Knockdown of FDX1 inhibits the proliferation of glioma cells. (**A**) The transfection efficiency of the FDX1 shRNA in U251 and SHG44 cells by qRT-PCR. (**B**) The CCK-8 assays showed the proliferation ability in the different FDX1 groups. (**C–F**) The EdU and colony formation assays revealed changes in cell viability after FDX1 alteration. Statistical analysis between two groups using the unpaired Student's t-test. *$p < 0.05$; **$p < 0.01$; ***$p < 0.005$.

Zhipeng Jiang: Resources, Formal analysis, Data curation. **Yirui Kuang:** Resources, Formal analysis, Data curation. **Haoxuan Huang:** Writing – review & editing, Data curation. **Weidong Liu:** Writing – review & editing. **Lei Wang:** Writing – review & editing, Software, Resources. **Zhaoqi Xin:** Writing – review & editing, Writing – original draft, Resources, Project administration, Methodology, Investigation, Formal analysis, Data curation, Conceptualization. **Binbin Wang:** Writing – review & editing, Resources, Project administration, Formal analysis, Data curation, Conceptualization. **Caiping Ren:** Writing – review & editing, Software, Resources, Project administration, Methodology, Investigation, Funding acquisition, Formal analysis, Data curation, Conceptualization. **Xingjun Jiang:** Writing – review & editing, Software, Resources, Project administration, Methodology, Investigation, Funding acquisition,
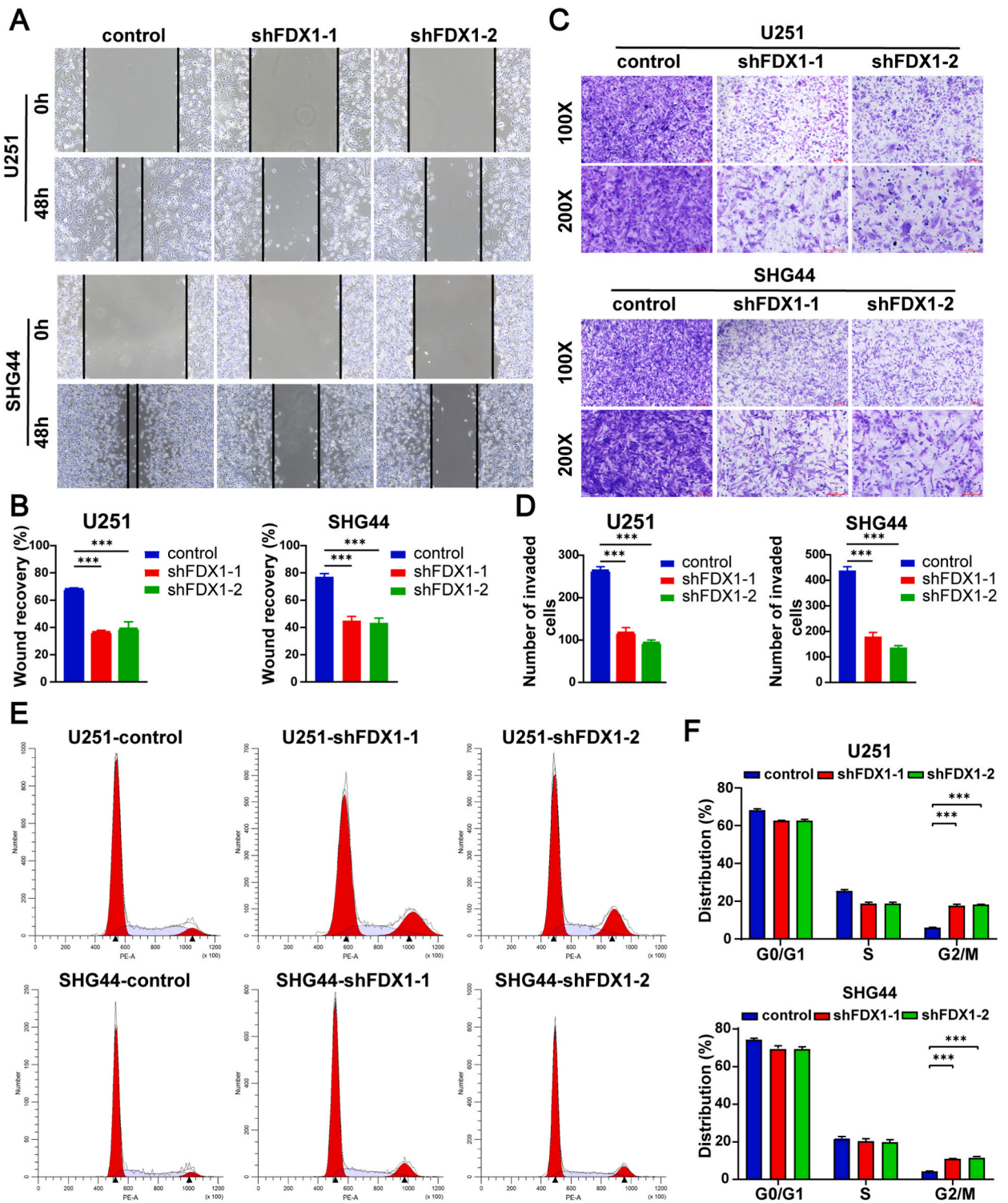
Fig. 11. Knockdown of FDX1 inhibits the migration, invasion ability and G2-M phase transition of glioma cells. (**A-B**) The wound healing assays indicated the invasive ability in the different FDX1 groups. (**C-D**) The transwell assays indicated the migratory ability in the different FDX1 groups. (**E-F**) Flow cytometry revealed changes in the cell cycle in the different FDX1 groups. Statistical analysis between two groups using the unpaired Student's t-test. $*p < 0.05$; $**p < 0.01$; $***p < 0.005$.

Formal analysis, Data curation, Conceptualization.

Declaration of competing interest

The authors declare that they have no known competing financial interests or personal relationships that could have appeared to influence the work reported in this paper.

Abbreviations

TCGA	The Cancer Genome Atlas
CGGA	Chinese Glioma Genome Atlas
GTEx	Genotype-Tissue Expression
TMA	Tissue Microarray
GBM	Glioblastoma Multiforme
LGG	Low Grade Glioma
WHO	World Health Organization Classification
IDH	Isocitrate Dehydrogenase
MGMT	O-6-Methylguanine-DNA Methyltransferase
TCA	Tricarboxylic Acid
ROC	Receiver Operating Characteristic
AUC	Area Under the Curve
OS	Overall Survival
DSS	Disease-Specific Survival
PFI	Progression-Free Interval
PCA	Principle Component Analysis
DEG	Differential Expression Gene
GO	Gene Ontology
KEGG	Kyoto Encyclopedia of Genes and Genomes
GSEA	Gene Set Enrichment Analysis
BP	Biological Processes
CC	Cellular Components
MF	Molecular Function
FDR	False Discovery Rate
NES	Normalized Enrichment Score
MAF	Mutation Annotation Format
CAFs	Cancer Associated Fibroblasts
TICs	Tumor-infiltrating Immune Cells
MCP	Microenvironment Cell Populations
TMB	Tumor Mutational Burden
TME	Tumor Microenvironment
qRT-PCR	Quantitative real-time PCR

Appendix A. Supplementary data

Supplementary data to this article can be found online at https://doi.org/10.1016/j.heliyon.2024.e26976.

References

[1] D.N. Louis, et al., The 2021 WHO classification of tumors of the central nervous system: a summary, Neuro Oncol. 23 (8) (2021) 1231–1251.
[2] T. Jiang, et al., CGCG clinical practice guidelines for the management of adult diffuse gliomas, Cancer Lett. 375 (2) (2016) 263–273.
[3] D.N. Louis, et al., The 2007 WHO classification of tumours of the central nervous system, Acta Neuropathol. 114 (2) (2007) 97–109.
[4] K. Ichimura, et al., IDH1 mutations are present in the majority of common adult gliomas but rare in primary glioblastomas, Neuro Oncol. 11 (4) (2009) 341–347.
[5] F. Guerrini, et al., Is it Worth considering multicentric high-grade glioma a surgical disease? Analysis of our clinical experience and literature review, Tomography 7 (4) (2021) 523–532.
[6] A. Grossen, et al., Physical forces in glioblastoma migration: a systematic review, Int. J. Mol. Sci. 23 (7) (2022).
[7] C. Bastianich, et al., Does local drug delivery still hold therapeutic promise for brain cancer? A systematic review, J. Contr. Release 337 (2021) 296–305.
[8] B.E. Kim, T. Nevitt, D.J. Thiele, Mechanisms for copper acquisition, distribution and regulation, Nat. Chem. Biol. 4 (3) (2008) 176–185.
[9] S. Majumder, et al., The role of copper in drug-resistant murine and human tumors, Biometals 22 (2) (2009) 377–384.
[10] X. Ren, et al., Overcoming the compensatory elevation of NRF2 renders hepatocellular carcinoma cells more vulnerable to disulfiram/copper-induced ferroptosis, Redox Biol. 46 (2021) 102122.
[11] N. Strushkevich, et al., Structural basis for pregnenolone biosynthesis by the mitochondrial monooxygenase system, Proc. Natl. Acad. Sci. U.S.A. 108 (25) (2011) 10139–10143.

[12] P. Tsvetkov, et al., Copper induces cell death by targeting lipoylated TCA cycle proteins, Science 375 (6586) (2022) 1254–1261.
[13] Z. Zhang, et al., FDX1 can impact the prognosis and mediate the metabolism of lung adenocarcinoma, Front. Pharmacol. 12 (2021) 749134.
[14] J. Zhang, et al., FDXR regulates TP73 tumor suppressor via IRP2 to modulate aging and tumor suppression, J. Pathol. 251 (3) (2020) 284–296.
[15] Q. Zhang, et al., Molecular mechanism underlying differential apoptosis between human melanoma cell lines UACC903 and UACC903(+6) revealed by mitochondria-focused cDNA microarrays, Apoptosis 13 (8) (2008) 993–1004.
[16] S. Stilgenbauer, et al., Molecular cytogenetic delineation of a novel critical genomic region in chromosome bands 11q22.3-923.1 in lymphoproliferative disorders, Proc. Natl. Acad. Sci. U.S.A. 93 (21) (1996) 11837–11841.
[17] K.C. Johnson, et al., Single-cell multimodal glioma analyses identify epigenetic regulators of cellular plasticity and environmental stress response, Nat. Genet. 53 (10) (2021) 1456–1468.
[18] X. Zhang, et al., Long non-coding RNA LPP-AS2 promotes glioma tumorigenesis via miR-7-5p/EGFR/PI3K/AKT/c-MYC feedback loop, J. Exp. Clin. Cancer Res. 39 (1) (2020) 196.
[19] W. Jia, et al., Effects of three-dimensional collagen scaffolds on the expression profiles and biological functions of glioma cells, Int. J. Oncol. 52 (6) (2018) 1787–1800.
[20] T.N. Schumacher, R.D. Schreiber, Neoantigens in cancer immunotherapy, Science 348 (6230) (2015) 69–74.
[21] J. Setton, et al., Synthetic lethality in cancer therapeutics: the next generation, Cancer Discov. 11 (7) (2021) 1626–1635.
[22] M.J. Mair, et al., Understanding the activity of antibody-drug conjugates in primary and secondary brain tumours, Nat. Rev. Clin. Oncol. 20 (6) (2023) 372–389.
[23] S. Kannan, et al., Gliomas: genetic alterations, mechanisms of metastasis, recurrence, drug resistance, and recent trends in molecular therapeutic options, Biochem. Pharmacol. 201 (2022) 115090.
[24] F. Sahm, et al., CIC and FUBP1 mutations in oligodendrogliomas, oligoastrocytomas and astrocytomas, Acta Neuropathol. 123 (6) (2012) 853–860.
[25] L. Wang, et al., High expression of cuproptosis-related gene FDX1 in relation to good prognosis and immune cells infiltration in colon adenocarcinoma (COAD), J. Cancer Res. Clin. Oncol. 149 (1) (2023) 15–24.
[26] H. Lu, et al., A novel oncogenic role of FDX1 in human melanoma related to PD-L1 immune checkpoint, Int. J. Mol. Sci. 24 (11) (2023).
[27] T. Wang, et al., Cuproptosis-related gene FDX1 expression correlates with the prognosis and tumor immune microenvironment in clear cell renal cell carcinoma, Front. Immunol. 13 (2022) 999823.
[28] V. Kannappan, et al., Recent advances in repurposing disulfiram and disulfiram derivatives as copper-dependent anticancer agents, Front. Mol. Biosci. 8 (2021) 741316.
[29] K.G. Daniel, et al., Copper-binding compounds as proteasome inhibitors and apoptosis inducers in human cancer, Front. Biosci. 12 (2007) 135–144.
[30] B. Maier, et al., A conserved dendritic-cell regulatory program limits antitumour immunity, Nature 580 (7802) (2020) 257–262.
[31] T. Shimamura, S.R. Husain, R.K. Puri, The IL-4 and IL-13 pseudomonas exotoxins: new hope for brain tumor therapy, Neurosurg. Focus 20 (4) (2006) E11.
[32] C. Neumann, A. Scheffold, S. Rutz, Functions and regulation of T cell-derived interleukin-10, Semin. Immunol. 44 (2019) 101344.
[33] M. Oft, IL-10: master switch from tumor-promoting inflammation to antitumor immunity, Cancer Immunol. Res. 2 (3) (2014) 194–199.
[34] Q. Duan, et al., Turning cold into hot: firing up the tumor microenvironment, Trends Cancer 6 (7) (2020) 605–618.
[35] A. Gieryng, et al., Immune microenvironment of gliomas, Lab. Invest. 97 (5) (2017) 498–518.
[36] A.B. Heimberger, et al., Incidence and prognostic impact of FoxP3+ regulatory T cells in human gliomas, Clin. Cancer Res. 14 (16) (2008) 5166–5172.
[37] Y. Qi, et al., Immune checkpoint targeted therapy in glioma: status and hopes, Front. Immunol. 11 (2020) 578877.
[38] R.G. Verhaak, et al., Integrated genomic analysis identifies clinically relevant subtypes of glioblastoma characterized by abnormalities in PDGFRA, IDH1, EGFR, and NF1, Cancer Cell 17 (1) (2010) 98–110.
[39] C.C. Smith, et al., Alternative tumour-specific antigens, Nat. Rev. Cancer 19 (8) (2019) 465–478.
[40] S. Jhunjhunwala, C. Hammer, L. Delamarre, Antigen presentation in cancer: insights into tumour immunogenicity and immune evasion, Nat. Rev. Cancer 21 (5) (2021) 298–312.
[41] R.L.Y. Ho, I.A.W. Ho, Recent advances in glioma therapy: combining vascular normalization and immune checkpoint blockade, Cancers 13 (15) (2021).
[42] L.A. Emens, et al., Cancer immunotherapy: opportunities and challenges in the rapidly evolving clinical landscape, Eur. J. Cancer 81 (2017) 116–129.